Applied Science and Engineering Progress, Vol. 20, No. 3, 2027, 8278

Research Article

Towards Smart Substations: A Cloud-Based Hybrid Deep Learning Model for Fault Detection and Predictive Maintenance of GIS Equipment

Ahmed Mohammed Merza
University of Babylon, College of Engineering Al-Musayab, Department of Energy and Renewable Energies Engineering, Department of Biomedical Engineering, College of Engineering, University of Warith Al-Anbiyaa, Karbala, Iraq

Ali Abdulhasan Rasool Al-Karaawi
College of Dentistry, University of Hilla, Babylon, Iraq

Assel Ali Hussein
Department of Physics, College of Science, University of Babylon, Babylon, Iraq

Ahmed Shaker Abdulaah
Department of Computer Techniques Engineering, Alsafwa University College, Karbala 56001, Iraq

Mohammed Abdul Azeez Yousif Alkhafaji, Ali Najim Abdullah* and Wael Abdulhasan Atiyah
General Company for Electrical Energy Transmission – Middle Euphrates Region, Ministry of Electricity, Babylon, Iraq

* Corresponding author. E-mail: alinajim0090@gmail.com DOI: 10.14416/j.asep.2026.08.012
Received: 10 May 2026 ; Revised: 27 June 2026 ; Accepted: 2 July 2026 ; Published online: 24 August 2026

Abstract
Gas-insulated substations (GIS) have become an important constituent of extra-high voltage (EHV) electrical systems because they are smaller and more efficient. Conversely, the conventional maintenance method, which usually relies on planned maintenance, can lead to unnecessary maintenance or sudden equipment failure. This research work is a holistic framework that would increase fault detection and proactive protection of GIS equipment. In the proposed design, a hybrid CNN–LSTM model processes multimodal sensor data (PD, temperature, SF_3, and environmental measures) for fault identification and predictive maintenance, while the cloud platform provides expandable storage, real-time analysis, and digital twin-based monitoring. Additionally, before switching operations, the DC main contact validation subsystem acts as a physical verification layer to verify conductor-path integrity. The updated manuscript highlights these components' complementary roles in improving GIS dependability, safety, and maintenance efficiency by clearly describing how they interact within a unified end-to-end architecture. The proposed framework achieves an average classification accuracy of 94.7%, with a macro-F1 score of 94.3% and an AUC of 0.965, demonstrating strong performance across multiple modalities. It also achieves a TPR of 0.88 at 1% FPR and an ECE of 2.7%, indicating reliable and well-calibrated detection. A real-world case study of a 132 kV GIS explosion in the Hilla West substation confirms that early warning indicators and pre-operational DC contact verification can effectively prevent failures, supporting the practicality and scalability of intelligent GIS monitoring systems.

Keywords: Hybrid CNN–LSTM, Cloud Computing, SF_6 gas, Predictive Maintenance, Smart Substation

1 Introduction

The power grid must function dependably to provide industrial progress, economic expansion, and the standard of living in the world. Substations are part of the grid to provide power flow control, voltage transformation, switching, and system protection. There has been an increasing reliance on EHV power plants capable of transmitting and distributing power over long distances with minimal losses as demand for electricity increases, especially in urban and industrial areas [1]. It benefits from the various insulation properties (GIS), which are capable of achieving them, and its small size, which is among the most important power stations, as SF_6 is used as an electrical insulator, which provides electrical insulation with high levels of safety, and the insulation strength is much greater than traditional air-insulated power systems. For this reason, the use of GIS is particularly attractive in areas with limited land use, dense urban areas, and environmentally sensitive areas [2].

Despite these advantages, GIS technology does have its drawbacks. While their components typically require less maintenance than conventional systems, they are still susceptible to unexpected problems and power outages. The most common problems include SF_6 gas leakage, which reduces the strength of the dielectric and causes physical damage; thermal stress, which results in confined hot spots; physical damage to switching devices; and partial discharges caused by voids or contaminants within the dielectric [3]. These issues are usually hard to detect until they occur, as GIS elements are enclosed in unbreakable containers. The consequences of EHV interruptions may be severe, with examples being extended power cutoffs, equipment damage, loss of money, and even risk to the safety of workers. Consequently, monitoring of system health and predictive maintenance is a topic of high research and industrial concern because of the extreme significance of GIS reliability [4].

In the past, the maintenance of the energy infrastructure and the GIS substations has either been performed in a preventive or corrective manner. When equipment is repaired or replaced only after its breakdown, this is a reactive maintenance approach called corrective maintenance. Even though the method has the advantage of cutting the costs of maintenance carried out regularly, it is very dangerous in systems that can easily wear and tear and cause an extensive spread of damage. On the other hand, preventive maintenance is founded on regular checks and repairs even when the equipment is not in good condition. Preventive maintenance, as much as it should be done, is inefficient [5]. Tearing down and repairing equipment may occur during good operation when preclinical maintenance is not always scheduled and may lead to unforeseen consequences. These have been substituted by condition-based maintenance (CBM) and predictive maintenance (PdM) [6]. CBM refers to a system that uses sensor data and diagnostic aids to assess equipment status when there are variations. The extension of this is to label the PdM, which applies analytics and machine learning to predict possible failure and estimate the equipment life. The digital transformation of power substations, i.e., the integration of smart electronics, Internet of Things (IoT) sensors, and sophisticated SCADA systems, has made predictive maintenance not only a possibility but a highly useful option as well [7].

This landscape has been transformed with the introduction of deep learning. Convolutional neural networks (CNNs), recurrent neural networks (RNNs), and long short-term memory (LSTM) structures are examples of deep learning techniques that can automatically learn discriminative features directly from raw data, from images to time series signals to mixed sensor streams [8]. CNNs can efficiently extract spatial and frequency features from two-dimensional inputs like phase-resolved partial discharge patterns or thermal images, while LSTMs and related architectures can model long-term temporal dependencies in continuous data like gas leak trends, load variations, or acoustic signals. The ability of hybrid networks that combine CNNs and LSTMs to capture both temporal and spatial aspects of analysis processes makes them highly effective. Therefore, hybrid deep learning networks can be well suited for predictive GIS maintenance, where heterogeneous data from multiple sources must be integrated to reliably detect faults and predict conditions [9].

Another challenge arises when applying this approach to deep learning models in substation maintenance. Many sensors, such as high-frequency partial discharge signals, infrared thermography, SF_6 gas sensors, humidity and temperature monitors, acoustic sensors, and SCADA event logs, record massive amounts of data when used with a GIS system [10]. Deep learning models therefore require significant computing resources to train and run on this data, as well as a scalable infrastructure for data storage. In substations, computing systems are often limited in capacity and unsuitable for this model [11].

A digital twin is a cloud computing concept that simulates and predicts equipment behavior using real-time GIS parameters and is fed actual operational data to enable predictive maintenance. The deep learning models applied on a cloud platform and made possible by real-time sensor data help in proactive maintenance scheduling, early fault detection, and real-time monitoring. Besides, remote cloud reliability and data security are beginning to be handled by the technology of cybersecurity. Further accuracy of the models can be felt in case the data is exchanged between the permitted enterprises and other substations [12]. In addition to data-based fault detection, the proposed system would also have an embedded DC primary contact checking module, which would be utilized to check the integrity of the GIS conductor path before switching operations. This inbuilt tester is used to measure contact resistance to provide a real-time safety check, which is not to operate under faulty or degraded contact conditions [13].

The current studies on GIS monitoring have extensively embraced the use of deep learning in partial discharge (PD) classification, especially the use of CNN-based models, which are highly accurate in controlled environments [14]. Additional time-frequency methods with spectrograms and convolutional neural networks also improve the extraction of features in non-stationary PD signals [15]. Moreover, predictive maintenance plans have been designed that aim at estimating the health of insulation and assisting in maintenance planning in GIS systems [16]. Machine learning with the integration of new sensors has enhanced monitoring of conditions by allowing the diagnosis of faults based on multi-source measurements [17]. What is more, cloud-based monitoring systems offer scalable data management and real-time analysis, but frequently do not have smart diagnostics and protection features [18]. These limitations underscore the importance of an integrated framework that integrates multimodal analysis and physical verification, as suggested in this work.

The objective of this research is to address the critical need for realistic, intelligent, practical, and scalable solutions for predictive maintenance of UHV in GIS substations. The research will run a hybrid deep learning architecture based on a cloud computing platform to connect with the richness of plant data and offer real-time analytics by combining the benefits of CNNs and LSTMs in fault detection and condition prediction [19]. The suggested system incorporates and makes use of environmental parameters, thermal images, PD signals, and SF_6 gas readings of the GIS system into one diagnostic model capable of forecasting equipment health, detecting normal and abnormal conditions, and giving early warnings of possible breakdowns. The use of a cloud-based AI model makes predictive maintenance more effective because it provides the option to access and store data on different GIS substations, scale computing resources, and enable remote monitoring. Therefore, the proposed system offers accuracy, reliability, and a considerable decrease in maintenance costs and downtimes, as compared to the traditional maintenance method. The model should also be experimentally checked with field-collected data sets and standard data.

The remainder of this paper is organized as follows. Section 2 presents the methodology (deep learning and cloud computing), Section 3 discusses the 132 kV GIS explosion case study, Section 4 introduces the proposed DC contact verification system, Section 5 presents results and discussion, and Section 6 concludes the paper.

2 Methodology

This study approach outlines the creation and implementation of a hybrid deep learning platform based on the cloud. The proposed AI model is built by using a fusion of LSTM and CNN in early fault identification and maintenance prediction using the operating conditions of equipment in EHV GIS substations. The process of model construction is broken down into a number of steps, which are data collection, preprocessing, cloud integration, model parameter training and optimization, performance evaluation, and ethical issues. Each of the stages is explained in the following subsections.

2.1 *Data acquisition*

Timestamps were used to synchronize PD signals, thermal images, and SF_6/environmental data collected from the same GIS equipment under identical operating conditions. Measurements obtained within the same time window were temporally aligned to form each multimodal sample. After preprocessing and normalization, the aligned data were integrated into unified multimodal instances representing specific equipment states (normal or abnormal). This synchronization ensures consistency across modalities and improves dataset reliability. The structure and composition of the multimodal dataset are summarized in Table 1.

The dataset used in this study consists of two primary sources: (i) field data collected from operational GIS substations and (ii) external/public reference datasets used to enhance model generalization. The field dataset includes PD signals, thermal images, and SF_6/environmental measurements

Table 1: Dataset used in model training and evaluation.

Modality	Description	Number of Samples	Classes	Sampling Rate / Resolution	Preprocessing Steps
Electrical signal (PD/AE waveforms)	Time-domain current and acoustic emission traces collected from GIS under various operational states	2,400	Normal, Corona, Surface, Internal	10 MHz / 8-bit	Band-pass filtering (100–800 kHz), normalization, segmentation (200 µs windows)
Thermal imagery	Infrared frames from substation thermal cameras covering busbars, insulators, and SF_6 tanks	1,600	Normal, Hotspot, Fault	320×240 pixels (8–14 µm band)	Histogram equalization, temperature calibration, and resizing
Environmental & SF_6 parameters	SF_6 concentration, humidity, pressure, and ambient/compartment temperature logs	2,400	Normal, Abnormal	1 Hz	Smoothing (rolling mean, 5-s window), missing-value imputation
Combined multimodal records	Synchronized signal, image, and environmental samples forming aligned training instances	1,200	Normal / Any-abnormal	—	Timestamp alignment, feature standardization
Test dataset (held-out)	An independent set of multimodal instances from separate equipment or time periods	400	Normal, Fault types	—	No augmentation; used for final evaluation only

Table 2: The normal operating limits of important values in a 132 kV GIS system.

Parameter	Normal Operation Range	Fault Condition Indicators	Notes
Gas Pressure (SF_6)	2.5 - 3.0 bar	Below 2.0 bar or above 3.5 bar	Low or high pressure can indicate leakage or a fault.
Gas Density (SF_6)	5.5 - 6.5 kg/m³	Below 5.0 kg/m³ or above 7.0 kg/m³	Low gas density suggests leaks, high indicates overpressure.
Temperature	-5°C to 40°C	Above 50°C or rapid fluctuations	Overheating may point to an internal fault or overload.
Partial Discharge (PD)	No discharge (0 pC)	> 100 pC (depending on equipment design)	Significant PD activity suggests insulation degradation.
Current (Load)	80% - 120% of rated current	Above 120% or below 30% of rated current	Overload or underload conditions point to faults or system misconfigurations.
Voltage	110 kV - 132 kV	Below 110 kV or above 132 kV	Voltage drop or surge indicates potential faults in the system.
Vibration	< 0.1 mm/s	> 0.2 mm/s	Excessive vibration can indicate mechanical failure.
Gas Temperature	20°C - 40°C	Above 50°C or rapid increases in temperature	High temperatures may suggest a fault causing overheating.
Leakage Detection	0%	> 2% SF_6 gas leakage rate	Any gas leakage beyond a threshold indicates a fault.

acquired under real operating conditions, while the external datasets provide additional labeled samples for similar fault categories.

To ensure consistency, all datasets were harmonized through a unified preprocessing pipeline, including normalization, resampling, and label standardization. Differences in sensor configurations, sampling rates, and operating environments were addressed using data alignment and scaling techniques. This integration enabled the construction of a consistent multimodal dataset suitable for training and evaluation.

Table 2 indicates the normal operating limits of important values in a 132 kV GIS system as well as a comparison with fault status indicators. The thermal imaging workflow was standardized by resizing images to 224×224 pixels. Temperature calibration was applied using radiometric scaling, followed by normalization and contrast enhancement. Data augmentation, including rotation, reflection, and scaling, improved generalization. Hotspot labels were assigned based on temperature thresholds and expert annotation, ensuring consistent identification of normal and abnormal thermal conditions.

2.2 *Data preprocessing*

A comprehensive preparation process is used to standardize inputs and improve data quality, as shown in Figure 1. Our model utilizes several key representations reflecting the heterogeneous nature of GIS datasets, including time-series environmental data, two-dimensional thermal images, and high-frequency PD/AE signals. The PD and AE signals were denoised using discrete wavelet transforms to suppress background noise and interference. The signals were then normalized to a fixed amplitude range and transformed into time–frequency spectrograms using the Short-Time Fourier Transform (STFT) with a Hamming window (256 samples, 50% overlap). Designed CNNs extract spectral and spatial features from these representations. Thermal images were resized to 224×224 resolution, normalized, and augmented using geometric and photometric transformations such as rotation, reflection, scaling, and brightness adjustment to improve generalization and reduce overfitting. Missing values in SF_6 and environmental measurements were interpolated using linear methods and normalized to the range [0,1]. Finally, all modalities were temporally synchronized using timestamps and segmented into fixed-length sequences (50 time steps) using sliding windows for LSTM modeling [20].

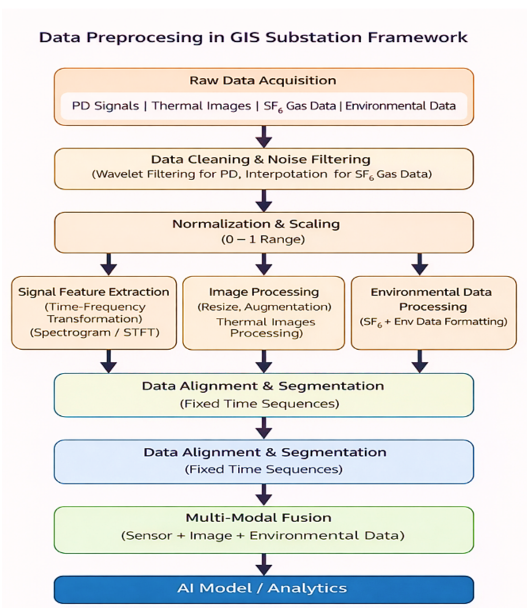

Figure 1: Data preprocessing coming from GIS system.

2.3 *Hybrid deep learning model design*

The architecture of the proposed hybrid model has been further detailed as show in Figure 2 to enhance reproducibility. The convolutional neural network (CNN) branch consists of three convolutional layers with 3×3 kernels and increasing filter depths of 32, 64, and 128, each followed by ReLU activation and max-pooling operations to extract spatial features from thermal and PD representations. The extracted feature maps are flattened and passed to fully connected layers for feature abstraction. In parallel, the temporal branch employs a stacked Long Short-Term Memory (LSTM) network with two layers comprising 64 and 32 units to model sequential dependencies in SF_6 and environmental data. A late-fusion strategy is implemented by concatenating features from both branches into a unified representation. The fused vector is processed through dense layers (128 and 64 neurons) with dropout regularization to prevent overfitting. Finally, a sigmoid classification head produces binary outputs corresponding to normal and abnormal conditions [21]. The multimodal fusion mechanism is implemented using a late-fusion strategy, where features extracted independently from each modality are combined at the feature level. The CNN branch processes PD and thermal data to extract spatial features, while the LSTM branch captures temporal patterns from SF_6 and environmental data. The outputs of both branches are concatenated to form a unified feature vector, which is then passed to fully connected layers for classification. The previously used term "gated fusion" has been removed to maintain consistency and clarity [22].

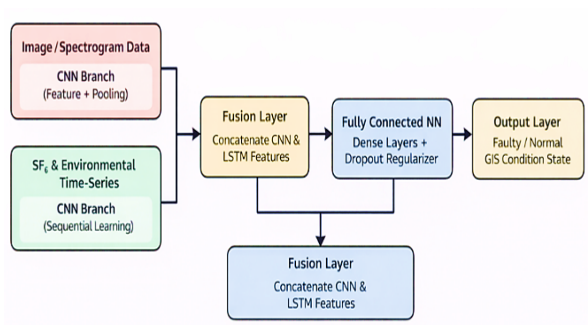

Figure 2: The hybrid CNN-LSTM deep learning network design.

2.4 *Cloud computing Integration*

The deep learning model is designed in a cloud computing environment, as shown in Figure 3, to enable immediate access, efficiency, and scalability while meeting the performance requirements for processing the large volume of data generated by GIS systems at substations. Sensor data are securely transmitted using MQTT and IEC 61850 protocols and stored in distributed cloud platforms such as AWS S3 or Azure Blob Storage, where large-scale multimedia data can be efficiently processed using flexible cloud infrastructure [23]. Model training is accelerated using high-performance cloud-based GPUs, reducing computational time and improving convergence efficiency. After training, the hybrid model is deployed as a lightweight cloud service accessible to substation engineers through a graphical user interface (GUI). The dashboard provides partial discharge patterns, real-time health indicators, and early warning alerts to support condition-based maintenance decisions. The deep learning model is continuously updated using operational data and can be simulated within the cloud environment, incorporating digital twin technologies. Once validated, the trained model can be deployed across multiple substations, ensuring scalability, consistency, and reliable performance in real-world applications [24].

2.5 *Model training and hyperparameter optimization*

The CNN–LSTM hybrid neural network is trained using supervised learning on operational GIS data and performs classification based on equipment condition as normal or abnormal. Prior to training, the dataset is analyzed to extract relevant indicators, including thermal hotspot patterns, SF_6 gas condition features, and partial discharge (PD) intensity levels, followed by preprocessing and normalization to ensure data consistency. During training, the model minimizes the categorical cross-entropy loss function using the Adam optimizer with an initial learning rate of 0.001. The training process is conducted for 100 epochs with early stopping applied to prevent overfitting, and a batch size of 64 is used. Dropout is set to 0.5, and L2 regularization is applied to enhance generalization capability. Hyperparameter tuning is performed using a grid search approach, optimizing key parameters such as learning rate, convolutional filters, and LSTM units, as summarized in Table 3. A five-fold cross-validation strategy ensures robustness, while dataset partitioning is performed at the equipment/event level. Cloud-based GPUs accelerate training convergence and computational efficiency.

Table 3: Model training and hyperparameter optimization parameters.

Parameter	Description / Setting
Learning paradigm	PD/AE signals, Thermal image, Env/SF_6 values, Multimodal binary
Training, validation, test split	75 %, 15 %, 10 %
Optimization algorithm	Adam optimizer
Initial learning rate	0.001
Learning rate scheduler	Step decay (×0.5 every 10 epochs)
Batch size	32 instances (per GPU worker)
Number of epochs	100 (max early stop at 15 epochs patience)
Loss function	Weighted categorical cross-entropy (class imbalance correction)
Regularization	L2 = 1×10^{-4} ; Dropout = 0.3
Data augmentation	Random noise injection (signals); random flip

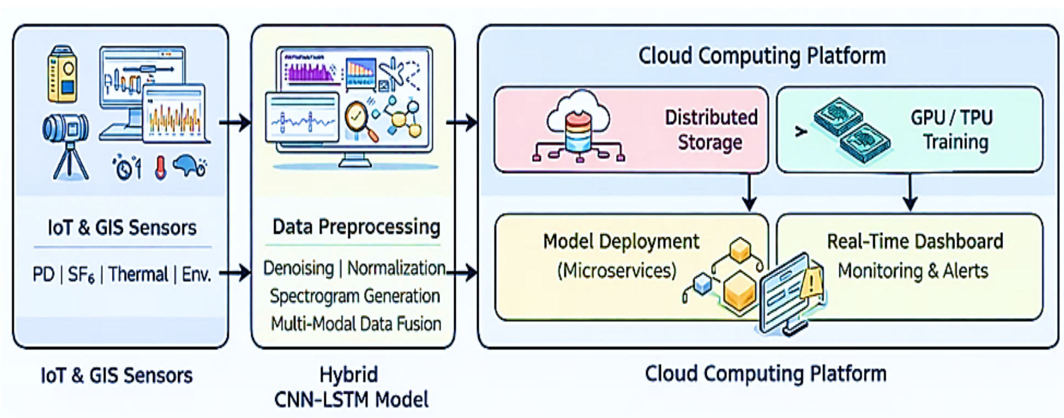

Figure 3: Cloud based for deep learning design of GIS system.

2.6 *Model evaluation*

The performance of the proposed system of CNN–LSTM integrated with a cloud framework was assessed utilizing a comprehensive group of statistical and metrics that can diagnose interpretability, reliability, and robustness across all performance states. The review centered on discrimination based on faults, prediction and classification accuracy of health trends, qualitative and quantitative analyses.

The accuracy and consistency of the model were measured on the standard performance indicators. The overall accuracy was calculated as in Equation (1):

$$Accuracy = \frac{(TP + TN)}{(TP + TN + FP + FN)} \quad (1)$$

Where $TP, TN, FP, and\ FN$ denote the counts of true positives, true negatives, false positives, and false negatives, respectively [25]. In order to measure per-class discrimination performance, the precision and recall of each class c were defined as Equation (2) and (3):

$$Precision_{(c)} = \frac{TP_{(c)}}{(TP_{(c)} + FP_{(c)})} \quad (2)$$

$$Recall_{(c)} = \frac{TP_{(c)}}{(TP_{(c)} + FN_{(c)})} \quad (3)$$

F1-score of their harmonic mean in Equation (4):

$$F1_{(c)} = \frac{2 \times (Precision_{(c)} \times Recall_{(c)})}{(Precision_{(c)} + Recall_{(c)})} \quad (4)$$

In order to have a balanced global indicator that is not dependent on the frequency of classes, we obtained the macro-averaged F1-score as in Equation (5):

$$Macro - F1 = \frac{1}{m} \times \sum_{(\mathrm{c=1 \to m})} \mathrm{F1_{(c)}} \quad (5)$$

Where m is the number of fault categories. The further evaluation of discriminative capacity at various thresholds was done by the Area Under the Curve (AUC) of Receiver Operating Characteristic (ROC) [26]. The AUC is the likelihood that the classifier places a positive sample on top of a negative sample and is defined as in Equation (6):

$$AUC = \int_0^1 TPR(FPR^{-1}(t))\, dt \quad (6)$$

Where the True Positive Rate $(TPR) = TP\,/\,(TP + FN)$ and the False Positive Rate $(FPR) = FP\,/\,(FP + TN)$. Higher values of AUC indicate increased separability between normal and faulty states. To make temporal predictions of equipment health trends, performance was measured in terms of Mean Absolute Error (MAE):

$$MAE = (\tfrac{1}{N}) \times \sum |y_i - \hat{y}_i| \quad (7)$$

In which y_i and $\hat{y}_i$ are the respective observed and forecasted values of the health index, and N is the number of time samples. Reduced MAE implies better forecasting of the trend [27]. The diagnostic visualization tools, such as confusion matrices, ROC curves and learning-curve analyses, were used to study class separability, systematic misclassifications and model stability. The comparative study of CNN, LSTM, and handcrafted-feature-based classifiers revealed that the hybrid CNN-LSTM model exhibited greater accuracy and macro-F1, and AUC-ROC, which underscores its usefulness in the detection process of both spatial and temporal characteristics of GIS fault behavior.

2.7 *Ethical and practical considerations*

In this research, a neural network model was developed within a cloud-based architecture to support real-time data processing and analysis. Consequently, strong emphasis was placed on data privacy and cybersecurity. All data are encrypted during transmission, processing, and storage, while access to cloud resources is strictly controlled through authentication protocols and role-based security policies. Potential cyber threats are mitigated using intrusion detection mechanisms, secure authentication procedures, and regular security audits. Protecting sensitive operational data is essential, as it is directly linked to critical infrastructure and national security. System reliability is further enhanced by generating early warnings that help prevent unnecessary switching operations and overload conditions, thereby reducing operational risks. In addition, environmental responsibilities are addressed by monitoring SF_6 gas conditions to ensure compliance with international standards. This helps minimize gas leakage and fire risks, contributing to sustainability and reduced environmental impact. Overall, ethical, security, and operational considerations are integrated to ensure that the proposed framework is not only technically effective but also safe, reliable.

3 Case Study: GIS 132 kV Explosion Incident

The case study centers on a 132 kV GIS system breakdown. It aims at elucidating the internal breakdown chain in the SF6 busbar compartment. Although GIS systems are considered to be reliable, there are latent problems that can arise, such as discharge of partial or contamination or contact degradation that will gradually reduce the insulation effectiveness without it being detected as a failure.

The accident was composed of internal dielectric failure and the gas breakdown and mechanical damage in the compartment. The pre-fault and post-fault conditions alongside the protection response were identified using visual inspection and disturbance record analysis. The case can be applied in predictive maintenance and preventive diagnostic intervention development for GIS equipment.

3.1 *Pre-fault condition analysis of 132 KV SF_6 busbar compartment*

A visual diagnosis of a 132 kV GIS busbar chamber, as shown in Figure 4, prior to a fault event showed no serious corrosion, melting, or deposition of decomposition products like aluminum fluoride (AlF_3), which showed that serious degradation of SF_6 had not yet taken place. Nonetheless, local electric field increases associated with small defects or faulty connections can trigger low-energy partial discharges, which slowly degrade the insulation and diminish dielectric strength with time. No visible byproducts indicate that the system is at a young age when it starts to degrade, and PD activity might not be represented in the form of visible byproducts. Failure of internal arcs may develop out of this latent condition unless it is carefully monitored. Hence, PD detection and SF_6 gas analysis should be constantly monitored to detect early degradation and avoid disastrous breakdown.

3.2 *After fault condition analysis of 132 kV SF_6 busbar compartment*

The 132kV GIS chamber post-failure examination, as shown in Figure 5, exhibited severe internal damage that included conductor erosion, pitting and carbonized-like residues, which was a long-term PD event that grew to be a high-energy internal arc. Its failure was precipitated by progressive degradation of insulation as a result of localized intensification of the electric field by surface defects, contamination, or inappropriate switching conditions, which resulted in uneven distribution of current and ultimate dielectric breakdown of SF_6 gas. The arc produced resulted in

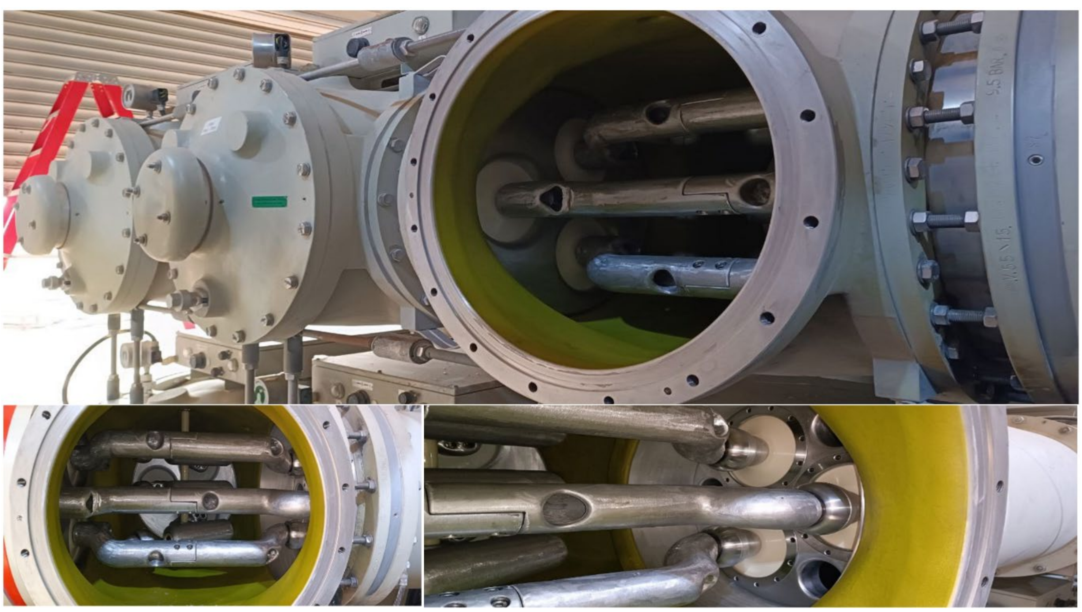

Figure 4: Pre-fault state of 132 KV SF_6 busbar compartment.

Figure 5: After fault state of 132 KV SF_6 busbar compartment.

extreme thermal and pressure loads, mechanical failure of the enclosure, deformation of metallic structures and movement of structural elements, including flanges and bolts. This latent degradation went unnoticed due to the lack of advanced monitoring systems and early warning signs would have been detected using techniques like PD detection, thermal images, and gas analysis. The case suggests that, now, more than ever, integrated monitoring solutions are necessary, with a hybrid cloud-edge deep learning system and DC contact check allowing for early fault detection, predictive maintenance, and preventing catastrophic GIS system failures.

3.3 *Disturbance record analysis and protection response*

A full interpretation of the disturbance record recorded during the 132 kV GIS busbar fault is given in this section using the recorded analog waveforms, binary protection signals, and the vector (phasor) diagrams.

3.3.1 Analog time diagram analysis

Figure 6 shows currents and voltages of the analog timescale (three-phase current and voltage) were in balance before the disturbance. The fault was entered in Babil 400 substation (400/132/11 kV) and connected with the West al Hilla substation (132/33 kV) on which a fault was observed. When the error is found, instantaneous values of currents on each phase are higher and the current on the neutral is smaller than on all phases. These values exceed the maximum overcurrent protection current of 1000 A that is a high-power fault. The type of fault may be determined as short circuiting between all phases and ground. The voltage waveforms are distorted and experience voltage breakdown. This is an indication that a short circuit occurred in the substation system next to this one, i.e., in the 132 kV GIS system and at the main Busbar No. 2.

3.3.2 Binary time diagram analysis

Figure 7 shows a binary time diagram of simultaneous ABB REL670 assertion of forward-start distance protection elements of all phases and earth fault detection follows. General distance protection and Zone-3 start signals are turned on and Zone-1 and Zone-2 are turned off. This means that it reached the Zone-3 with the apparent impedance only. The second Zone-3 trip ended up in protection operation and auto-reclose blocking. The temporality of the fault is shown by the short statement periods of the signals.

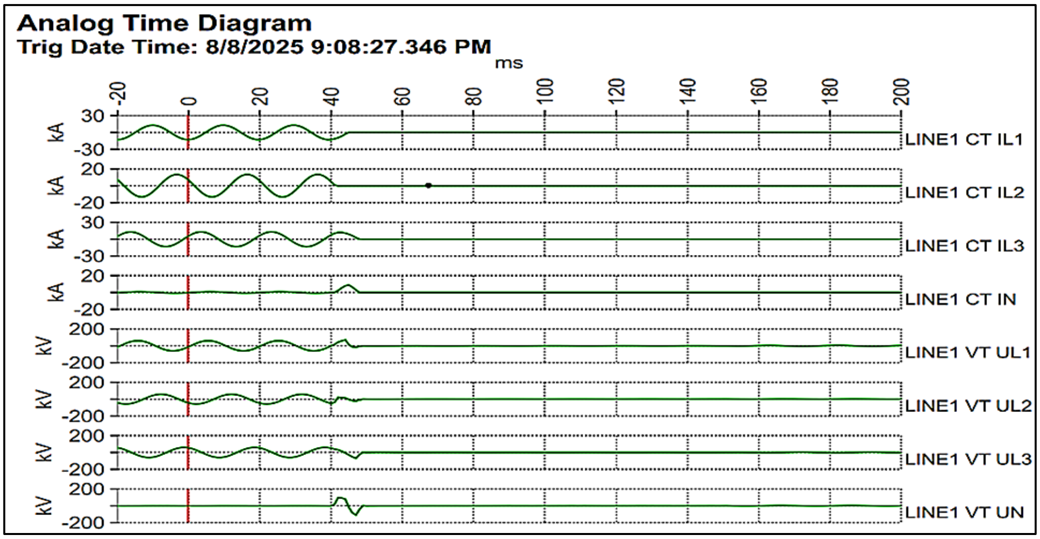

Figure 6: The analog timescale of currents and voltages during fault.

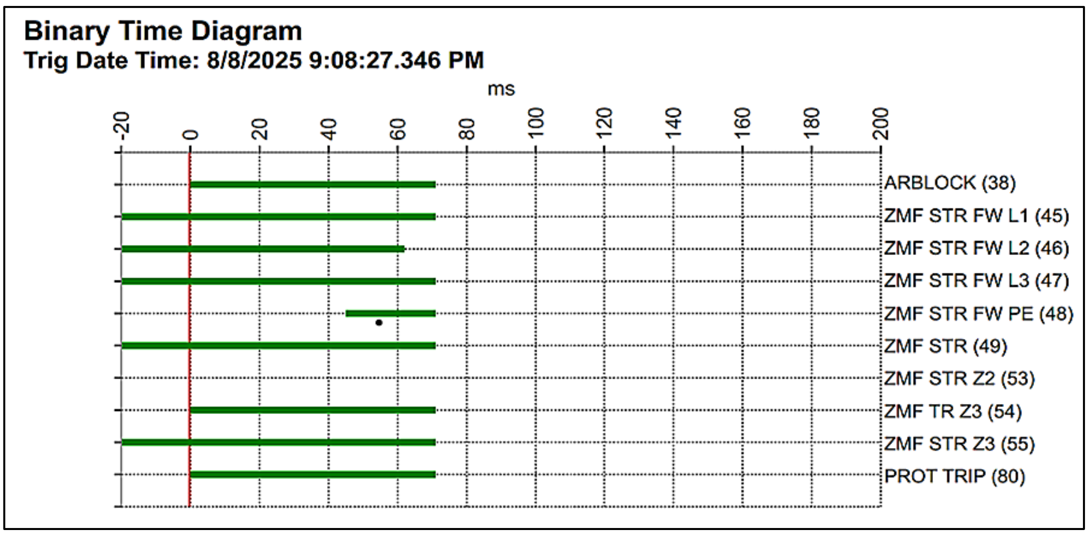

Figure 7: The binary time diagram of protection device performance during fault.

3.3.3 Vector (phasor) diagram analysis

Figure 8 in this incidence in the vector diagrams indicates that the currents are angularly varied and are therefore turbulent in nature and as such, the angular variation of the currents is harsh. There is a neutral current element, which is very small relative to the phase currents, whereas the actions of a ground fault, in which the zero-sequence components are dominant, are the opposite. The voltage vectors are not broken and distorted and the neutral voltage is at a reduced value, which also does not signify a line-to-ground fault. Therefore, the fact that there are several stages and the current is much higher than the overcurrent limit of 1000 A shows that the fault was a multiphase internal arc fault, and most probably that the fault was a phase-to-phase fault or phase-to-ground fault, which has taken place in the gas-insulated busbar compartment

3.3.4 Overall Interpretation

The parallel analysis proves the comparison between short-energy and high-energy internal GIS fault that

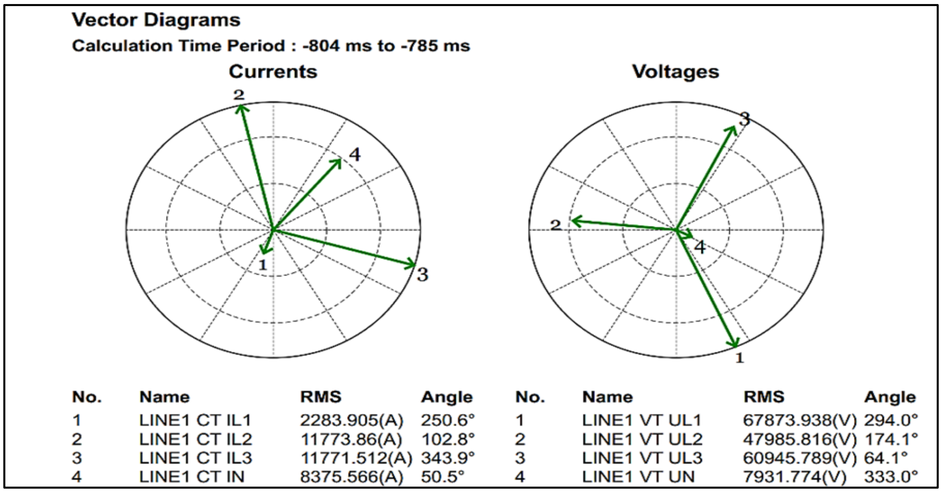

No.	Name	RMS	Angle	No.	Name	RMS	Angle
1	LINE1 CT IL1	2283.905(A)	250.6°	1	LINE1 VT UL1	67873.938(V)	294.0°
2	LINE1 CT IL2	11773.86(A)	102.8°	2	LINE1 VT UL2	47985.816(V)	174.1°
3	LINE1 CT IL3	11771.512(A)	343.9°	3	LINE1 VT UL3	60945.789(V)	64.1°
4	LINE1 CT IN	8375.566(A)	50.5°	4	LINE1 VT UN	7931.774(V)	333.0°

Figure 8: The vector diagrams of voltages and currents during fault.

has multiple phases and the single-line to ground fault, which is simple. The fault caused temporary but intense phase currents of higher than overcurrent settings and rapidly died off because of arc instability and enclosure effects. This is what makes no long-term operation of the differentiation protection and clearance of the fault to be performed by auxiliary Zone-3 distance protection. The results indicate that internal GIS arc faults may not be regarded as classical faults and require to undergo waveform, logic and physical analysis.

4 Proposed Solution: Automatic DC Primary Contact Verification System for GIS

This work suggests the implementation of an automatic DC primary contact verification system within GIS switching operations to verify the integrity of the main current path prior to energization, as shown in Figure 9. A DC is passed through the busbar, disconnectors and circuit breaker contacts and the voltage drop across the contacts is measured to determine contact resistance by Ohm's law (R=V/I). The resistance is calculated and compared to predefined thresholds, which is an indication of the condition of the conductive path as shown in Figure 10. When the value falls within acceptable limits, then the switching operation takes place; otherwise, an alarm is raised and the operation is inhibited. This will allow identifying bad contacts early and provide a protective layer that prevents, which greatly increases the safety and reliability of GIS substations.

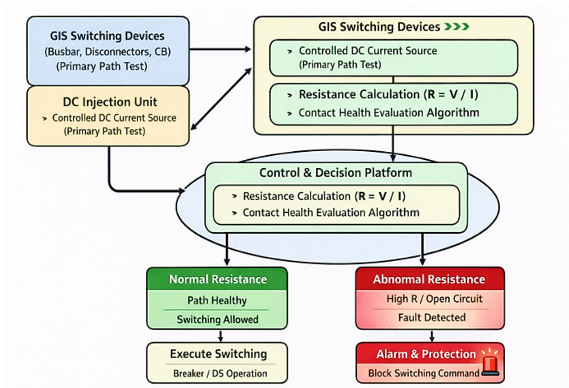

Figure 9: Operation steps of automatic dc primary contact verification system.

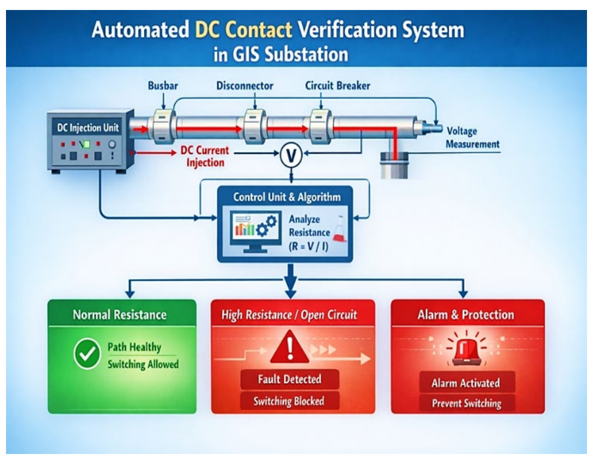

Figure 10: The design of automatic DC primary contact verification system.

5 Results and Discussion

In this section, we present the results of implementing a proposed multimodal model in a hybrid environment combining edge and cloud computing for real-time fault diagnosis of power substations, specifically within the GIS system, and for preventing catastrophic failures, as demonstrated in the West Hilla 132/33 kV substation incident. The model utilized edge devices for light preprocessing and data collection, put on a 132 kV GIS system, while the cloud platform enabled full integration of multimodal data and advanced analytics. The deep learning model of the GIS system was trained on a group of sensor data (electrical, vibration, and thermal), providing accurate classification of GIS fault types. The primary status detection of 132 kV GIS of the West Hilla 132/33 kV substation is carried out by the edge devices, which also reduce data transfer to the cloud by concentrating on important operational data and eliminating repetitive and routine information. Finally, the cloud platform collects multimodal data, performs in-depth analysis, and establishes the primary classification of sub-fault types, providing a comprehensive diagnosis and avoiding any incident such as the West Hilla 132/33 kV substation. The edge and cloud computing processes were compared to evaluate the model's performance and feasibility for real-time applications. Challenges such as sensor data variability and the need for more diverse training datasets of GIS substations for rare faults have been diagnosed. Future work will focus on enhancing data uniformity at the edge computing level and improving the GIS fault detection models to keep the equipment and to achieve reliability and accuracy under harsh conditions.

5.1 *Learning Curves*

The training-verification accuracy and training-verification loss graphs provide a complete picture of the performance of the CNN-LSTM model for the 132 kV GIS. The training and verification accuracy increases across training cycles, with the verification accuracy reaching a peak of approximately 0.93 as shown in Figure 11. The loss curves as shown in Figure 12 display a rapid decline during the first ten cycles. The model has reached the required accuracy, as both training and verification accuracy rose with each cycle, approaching 1 for training accuracy and reaching approximately 0.9 for verification accuracy, indicating good generalization. The loss graph shows that both training and verification losses reduced over time, but the training loss reduced more rapidly, indicating a better fit to the training data. It can also be concluded that the model does not suffer from over-allocation by observing the small gap between training loss and validation loss. Additionally, the model effectively generalizes from noting that verification loss and accuracy follow similar training trends. Verification performance can be enhanced by making further settings so that the model learns well from the data.

5.2 *Confusion Matrix Analysis*

The results of the confusion matrix give an evaluation of the predictive accuracy of the GIS 132kV classification model in its various operation states.

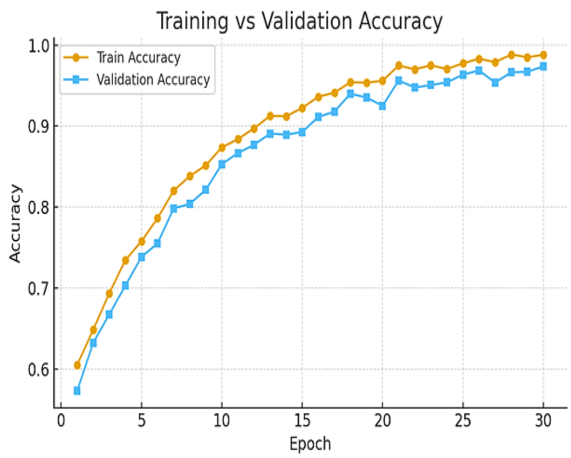

Figure 11: The training and verification curves.

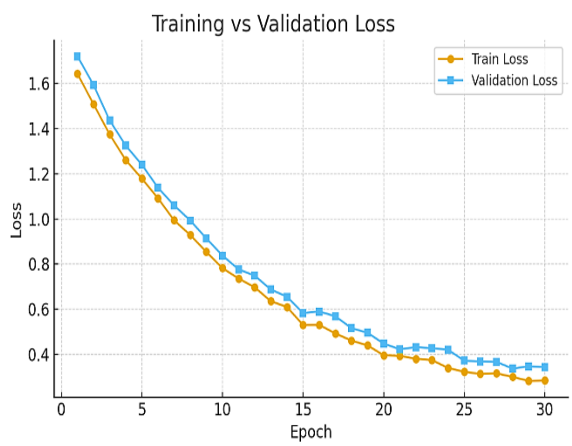

Figure 12: The training and verification loss curves.

In matrices, the diagonal numbers indicate correct classifications, and the non-diagonal numbers indicate incorrect classifications. In a case in point, the standard matrix of the group of the partial discharge states indicates that the model works, but it has issues in distinguishing between surface and interior states, normal states and other states, as shown in Figure 13. Similarly, within the thermal imaging classification as shown in Figure 14, the model has a challenge in differentiating between cracks and hot spots. SF_6 gas and environment classification, as shown in Figure 15, has a balanced prediction but there are some off-diagonal values. Finally, the multimodal matrix, as shown in Figure 16, shows that it has a high level of performance in the distinction between normal and abnormal states with only a few false classifications.

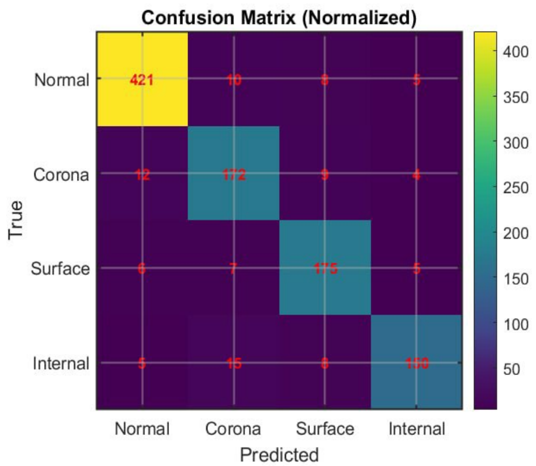

Figure 13: Partial discharge confusion matrix.

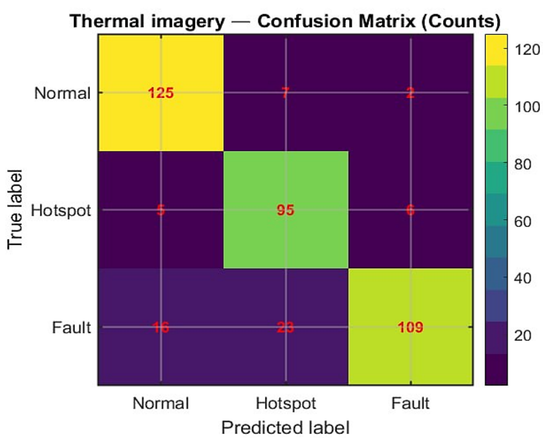

Figure 14: Thermal image confusion matrix.

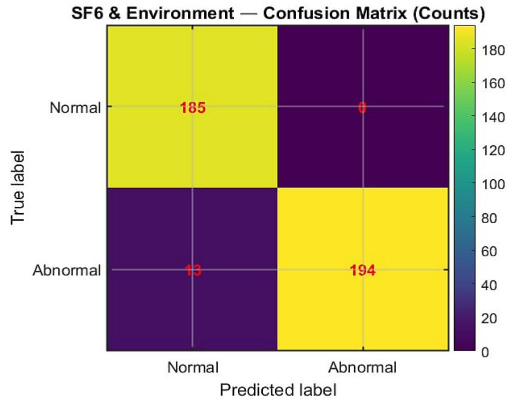

Figure 15: SF_6 and environment confusion matrix.

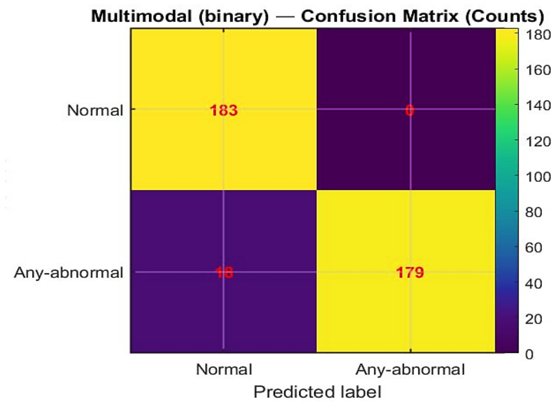

Figure 16: SF_6 and environment confusion matrix.

5.3 *DC injection test results*

Table 4 provides the comparison of the detectors of each modality on the same set of metrics which explains why the multimodal (gated fusion) model is the best to use in deployment. AUC (ROC) is a measure of quality at any threshold; a value of above one indicates that the model is more consistent in terms of its ability to distinguish between the normal and Faulty (maximum AUC is fusion). PR-AUC is suited to the abnormal cases and most practicable in the case where the rate of faults is not high; the optimal PR-AUC of fusion indicates less rate of faults and a lesser false-alarm rate. General accuracy is accuracy but it may not give a balanced performance of the classes; we have also reported Macro-F1, the average of individual-class F1, displaying balanced performance, best performance, in this case, is in PD/AE and Thermal, fusion

Table 4: The comparison of the detectors for each model.

Model / Modality	Task	AUC (ROC)	PR-AUC	Acc (%)	Macro-F1	TPR@1% FPR	ECE (%)
PD/AE (CNN-LSTM)	4-class (OvR avg)	0.953	0.941	94.0	93.5	—	3.0
Thermal (CNN-LSTM)	3-class (OvR avg)	0.948	0.936	93.6	93.0	—	3.2
Env/SF_6 (CNN-LSTM)	Binary	0.972	0.965	95.1	95.0	0.86	2.5
Multimodal (Gated Fusion)	Binary	0.985	0.977	96.2	95.6	0.90	2.1
Average	—	0.965	0.955	94.7	94.3	0.88	2.7

is best. There is also 1% FPR (true positive rate, with false alarm rates limited to 1%): the greater the value, the worse performance with strict alarm policy, once again fusion prevails, and Env/SF_6 model is strong at slow-varying anomalies. The ECE (Expected Calibration Error) is a measure of how well probabilities and the true state of affairs agree; a smaller ECE indicates that the scores may be directly mapped onto risk/maintenance decision- the low ECE of fusion implies that thresholding may be done dependably. PD/AE and Thermal models are correct in their respective ability, but fused model is the most appropriate in terms of detecting and infrequent fault recall, and so is the most reliable in terms of confidence scores, and so is the primary source of alarm, and unimodal models are complementary monitors.

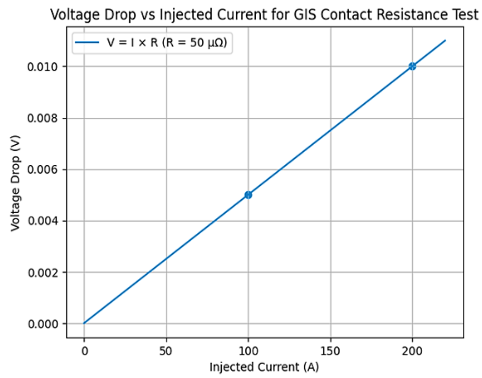

Figure 17: Voltage and current across GIS contact.

5.4 *DC injection test results*

The results of the DC injection test, as shown in Figure 17 indicate that the injected current has a direct relationship with the voltage drop across GIS contact path. One instance is that a 100 A injected current will produce a voltage drop of about 5 mV. When injecting a contact, a 10 mV change is seen with the doubling of injection current to 200 A with a contact resistance of 50 µ ohms. These results prove that this law of Ohm can be used in the measurement.

They also demonstrate that the more the injection currents, the better the measurement is to detect the contact resistance in GIS equipment at the micro-ohm level. The DC primary injection test was conducted on the GIS busbar conductor path with current levels of 100 A and 200 A. The equivalent resistance of the tested path was measured and was found to be 278 $\mu\Omega$.

Therefore, the voltage drop across the conductor was calculated as 27.8 mV with 100 A current and 55.6 mV with 200 A current, respectively, according to the calculated resistance. The results obtained show that there is a direct correlation between voltage and current utilized, and this is expected based on Ohm's law. Thus, this measurement demonstrates that the proposed DC verification technique can successfully and reliably detect contact resistance in GIS busbar.

5.5 *Comparative analysis of existing approaches*

Table 5 summarizes the key characteristics of existing GIS monitoring and partial discharge (PD) detection approaches and compares them with the proposed integrated framework. As shown, signal-based and spectrogram-based deep learning methods achieve high accuracy in controlled environments but are limited by their reliance on single-modality data and sensitivity to noise. Similarly, predictive maintenance and sensor-based machine learning approaches enhance fault detection capabilities; however, they often lack deep learning integration and do not include mechanisms to verify the physical integrity of the system. Cloud-based platforms provide scalability, distributed computing resources, and real-time data management; however, many existing systems remain focused on data storage and monitoring without incorporating advanced analytics, intelligent diagnostics, or integrated protection mechanisms. In contrast, the proposed architecture integrates multimodal data sources, including PD signals, thermal images, SF_6 gas measurements, and environmental features, within a unified CNN–LSTM classification framework supported by cloud computing. The cloud platform enables centralized

Table 5: The comparison recently works with the proposed integrated framework.

#	Approach (Paper Archetype)	Key Reference	Inputs / Modality	Core Model / System	Strengths	Limitations	Comparison with Proposed Framework
1	Signal-based Deep Learning for PD (CNN-based)	[14]	PRPD/PD signal data	CNN-based deep learning	High accuracy in PD classification; effective feature learning	Sensitive to noise; lacks environmental and physical context	Improved robustness using thermal, SF_6, and environmental data
2	Time–Frequency Deep Learning for PD (Spectrogram-based CNN)	[15]	UHF/PD signals → time–frequency images	2D-CNN	Effective feature extraction from non-stationary signals; improved classification accuracy	Requires stable signal acquisition; still single-modality	Proposed system enhances reliability using multimodal sensing (thermal + SF_6 + environment)
3	GIS-Based Predictive Maintenance for Electrical Insulators	[16]	Insulation condition data, PD indicators	Predictive maintenance model (data-driven)	Enables early fault prediction and maintenance planning	Focused on insulation; lacks multimodal integration and protection layer	Proposed system extends to full GIS monitoring with AI, multimodal data, and DC verification
4	Integration of Novel Sensors and Machine Learning for Predictive Maintenance	[17]	Multi-sensor data (thermal, electrical, environmental)	Machine learning-based predictive maintenance	Combines sensing and ML for improved fault detection	Limited deep learning and lacks physical verification (contact integrity)	Proposed system enhances with deep learning (CNN–LSTM), multimodal fusion, and DC contact verification
5	Cloud-Based Monitoring and Management Platform for Electrical Equipment	[18]	Sensor data streams from electrical equipment	Cloud-based monitoring and management system	Real-time monitoring, centralized data management, scalable deployment	Limited fault classification intelligence; lacks integrated protection mechanisms	Proposed system extends cloud capability by integrating AI-based diagnostics and DC contact verification for proactive protection
6	Proposed Integrated Framework	*(This work)*	PD signals + Thermal + SF_6 + Environmental data + DC injection	CNN + LSTM + DC contact verification + Cloud analytics	High accuracy (94.3%), robust performance, predictive + protective capability	Higher system complexity; requires sensor integration	Unified solution combining fault detection, prediction, and pre-operational safety verification

data aggregation from multiple substations, high-performance model training using GPU acceleration, and real-time inference through edge–cloud collaboration. In addition, it supports secure data handling, scalable storage, and efficient model updates across distributed systems. More importantly, the framework incorporates a DC primary contact verification system that ensures the electrical integrity of the GIS conductor path prior to switching operations. This integration of cloud-enabled intelligence with physical verification provides a comprehensive, robust, and safe solution for real-world GIS monitoring applications.

6 Conclusion

This paper presented an elaborate structure, which could be used in intelligent monitoring and proactive protection of gas-insulated switchgear (GIS). This method is a cloud-based hybrid deep learning model that consists of an automated DC primary contact verification system. The suggested methodology addresses the limitations of the traditional maintenance procedures because it allows not only predicting faults based on data but also checking the electrical conduction path before the operations. There was a high level of accuracy in detecting abnormal conditions using the hybrid CNN-LSTM model, in which multimodal sensor data was used with a classification accuracy of 94.3%. Moreover, cloud integration offered scalability, real-time processing and guaranteed reliable system performance. The effectiveness of the system was confirmed by a case study of a 132 kV GIS explosion incident. It proved that early warning signs such as the partial discharge activity, thermal anomalies, and SF6 gas decomposition can be effectively detected before a failure takes place. Moreover, the proposed DC injection system is a practical preventative control in that it establishes contact integrity before energization, thereby discouraging the possibility of internal failures due to high-resistance connections or open circuits. Taken together, the results suggest that the combination of the use of artificial intelligence and physical verification techniques is a powerful and easily implementable solution with developing predictive maintenance to enhance the reliability of the GIS. Future studies might focus on the expansion of the data, the addition of other diagnostic features, and the implementation of the system in real-time working substations to further confirm it.

Acknowledgments

The authors would like to express their sincere gratitude to all individuals who contributed to the preparation of this work. We extend special thanks to the General Company for Electricity Transmission/Middle Euphrates Region for their support and assistance during the research. The authors also acknowledge the individuals who provided technical guidance, language editing, and proofreading support.

Author Contributions

A.N. contributed to conceptualization, investigation, and methodology, as well as writing—original draft preparation. A.N. also contributed to data curation, review, editing, and funding acquisition. All authors have read and agreed to the published version of the manuscript.

Conflicts of Interest

The authors declare no conflict of interest.

Declaration of generative AI and AI-assisted technologies in the writing process

The authors utilized the ChatGPT tool to enhance the language and readability of the manuscript.

References

[1] N. Zebouchi and M. A. Haddad, "A review on real-size epoxy cast resin insulators for compact high voltage direct current gas insulated switchgears (GIS) and gas insulated transmission lines (GIL)—Current achievements and envisaged research and development," *Energies*, vol. 13, no. 23, p. 6416, Dec. 2020, doi: 10.3390/en13236416.

[2] A. Ymeri, N. Krasniqi, G. Kicaj, and D. Morina, "Advantages of a gas insulated substation (GIS)," in *Proceeding of UBT International Conference*, 2023, doi: 10.33107/ubt-ic.2023.53.

[3] T. Li, Q. Xu, K. Gao, Z. Yuan, J. Chen, and C. Li, "Review of insulation defect detection methods for a gas-insulated switchgear," Energies, vol. 19, no. 6, Art. no. 1491, Mar. 2026, doi: 10.3390/en19061491.

[4] Q. Wang, Z. He, S. Lin, and Z. Li, "Failure modeling and maintenance decision for GIS equipment subject to degradation and shocks," *IEEE Transactions on Power Delivery*, vol. 32, no. 2, pp. 1079–1088, Apr. 2017, doi: 10.1109/TPWRD.2017.2655010.

[5] D. Olojede, S. King, and I. Jennions, "Application of machine learning in power grid fault detection and maintenance," Energy Informatics, vol. 8, no. 1, Sep. 2025, doi: 10.1186/s42162-025-00574-w.

[6] Y. A. M. Alsumaidaee, C. T. Yaw, S. P. Koh, S. K. Tiong, C. P. Chen, and K. Ali, "Review of medium-voltage switchgear fault detection in a condition-based monitoring system by using deep learning," *Energies*, vol. 15, no. 18, p. 6762, Sep. 2022, doi: 10.3390/en15186762.

[7] K. Sundsgaard, "Predictive maintenance of medium voltage cable networks using machine learning," M.S. thesis, Technical University of Denmark, 2025, doi: 10.11581/e39dacea-e69a-4398-a8ed-68b3e0cfc96e.

[8] J. Xu, "GIS equipment status assessment method for substations based on multi-frequency signal processing," *International Journal for Housing Science and Its Applications*, vol. 46, no. 4, pp. 5978–5990, 2025. doi: 10.70517/ijhsa464435.

[9] P. D. Rocha, F. J. P. Lopes, and L. A. Da Silva Cruz, "Automating electrical grid asset inspection: From current challenges to future directions," *IEEE Access*, vol. 13, pp. 201392–201438, 2025, doi: 10.1109/ACCESS.2025.363 6718.

[10] W. Chi, T. Wang, J. Zhang, Z. Wang, and C. Zhang, "Full-life-cycle management of high-voltage bushings based on digital twin: Typical scenarios, core technologies, and research prospects," *Energies*, vol. 18, no. 23, p. 6343, Dec. 2025, doi: 10.3390/en18236343.
[11] T. Ji, Z. Liu, X. Zhuang, Q. Li, L. Zhang, and Q. H. Wu, "Advancing GIS operational monitoring: A novel voiceprint recognition method using Grassmann manifold and multi-kernel functions," *IEEE Transactions on Power Delivery*, vol. 39, no. 5, pp. 2894–2907, Oct. 2024, doi: 10.1109/TPWRD.2024.3448354.
[12] K. Sekar, M. S. Nattar, P. Muthukamatchi, N. Ranganathan, and S. Srithar, "Integrating machine learning and IoT for real-time PdM in industrial ecosystems: A case study analysis citation," *International Journal of Research in Industrial Engineering*, vol. 14, no. 2, pp. 385–409, 2025, doi: 10.22105/riej.2025.502596.1531.
[13] H. Koch et al., "Operation and maintenance," in *Gas Insulated Substations*, H. Koch, Ed. Hoboken, NJ, USA: Wiley, Dec. 2021, pp. 325–370, doi: 10.1002/9781119623632.ch7.
[14] W. Hu, J. Li, X. Liu, and G. Li, "Partial discharge fault identification method for GIS equipment based on improved deep learning," *The Journal of Engineering*, vol. 2024, no. 5, May 2024, doi: 10.1049/tje2.12386.
[15] Y. Sun et al., "Partial discharge pattern recognition of transformers based on MobileNets convolutional neural network," *Applied Sciences*, vol. 11, no. 15, p. 6984, Jul. 2021, doi: 10.3390/app11156984.
[16] A. Jafari, M. K. Azad, A. M. Zanjani, and M. A. Fatideh, "GIS-based predictive maintenance for electrical insulators," in *Proceeding of 2025 29th International Electrical Power Distribution Conference (EPDC)*, Tehran, Iran, 2025, pp. 1–6, doi: 10.1109/EPDC67173.2025.11278249.
[17] M. W. Hoffmann *et al.*, "Integration of novel sensors and machine learning for predictive maintenance in medium voltage switchgear to enable the energy and mobility revolutions," *Sensors*, vol. 20, no. 7, p. 2099, Apr. 2020, doi: 10.3390/s20072099.
[18] L. Yunyang, W. Lixiang, and Z. Yang, "Cloud-based monitoring and management platform for electrical equipment," in *Proceeding of 2025 IEEE 3rd International Conference on Image Processing and Computer Applications (ICIPCA)*, Shenyang, China, 2025, pp. 1995–1998, doi: 10.1109/ICIPCA65645.2025.11138900.
[19] S. Pan, W. Zhang, Y. Ma, Y. Su, and W. Huang, "Pattern recognition of GIS partial discharge based on UHF signal characteristics," *Electronics*, vol. 15, no. 5, p. 1096, Mar. 2026, doi: 10.3390/electronics15051096.
[20] A. Moradzadeh, H. Teimourzadeh, B. Mohammadi-Ivatloo, and K. Pourhossein, "Hybrid CNN-LSTM approaches for identification of type and locations of transmission line faults," *International Journal of Electrical Power & Energy Systems*, vol. 135, p. 107563, Feb. 2022, doi: 10.1016/j.ijepes.2021.107563.
[21] Y. A. M. Alsumaidaee *et al.*, "Fault detection for medium voltage switchgear using a deep learning hybrid 1D-CNN-LSTM model," *IEEE Access*, vol. 11, pp. 97574–97589, 2023, doi: 10.1109/ACCESS.2023.3294093.
[22] T. Liu, J. Yan, Y. Wang, Y. Xu, and Y. Zhao, "GIS partial discharge pattern recognition based on a novel convolutional neural networks and long short-term memory," *Entropy*, vol. 23, no. 6, p. 774, Jun. 2021, doi: 10.3390/e23060774.
[23] A. Aleran, H. Almukhalfi, A. Noor, R. Alluhaibi, A. Hafez, and T. H. Noor, "An IoT-based predictive maintenance framework using a hybrid deep learning model for smart industrial systems," *Computers, Materials and Continua*, vol. 86, no. 3, Jan. 2026, doi: 10.32604/cmc.2025.070741.
[24] S. Rana, "AI-driven fault detection and predictive maintenance in electrical power systems: A systematic review of data-driven approaches, digital twins, and self-healing grids," *American Journal of Advanced Technology and Engineering Solutions*, vol. 1, no. 1, pp. 258–289, Feb. 2025, doi: 10.63125/4p25x993.
[25] N. Q. Minh, N. T. Khiem, and V. H. Giang, "Fault classification and localization in power transmission line based on machine learning and combined CNN-LSTM models," *Energy Reports*, vol. 12, pp. 5610–5622, Nov. 2024, doi: 10.1016/j.egyr.2024.11.061.
[26] F. M. Almasoudi, "Grid distribution fault occurrence and remedial measures prediction/forecasting through different deep learning neural networks by using real time data

from Tabuk city power grid," *Energies*, vol. 16, no. 3, p. 1026, Jan. 2023, doi: 10.3390/en16031026.

[27] T. Li et al., "Durative monitoring of sulfur hexafluoride characteristic gases under hydrogen interference using a Time2Vec-encoded CNN–Transformer–LSTM model based on a heterogeneous gas sensor array," *ACS Sensors*, vol. 10, no. 11, pp. 8809–8820, Oct. 2025, doi: 10.1021/acssensors.5c02740.